EPJ Web of Conferences **3**, 05003 (2010)
DOI:10.1051/epjconf/20100305003

A novel treatment of the proton-proton Coulomb force in proton-deuteron Faddeev calculations

H. Witała[1,a], J. Golak[1], R. Skibiński[1], and W. Glöckle[2]

[1] M. Smoluchowski Institute of Physics, Jagiellonian University, PL-30059 Kraków, Poland
[2] Institut für theoretische Physik II, Ruhr-Universität Bochum, D-44780 Bochum, Germany

Abstract. We present resently introduced novel approach to include the proton-proton (pp) Coulomb force into the momentum space three-nucleon (3N) Faddeev calculations. It is based on a standard formulation for short range forces and relies on a screening of the long-range Coulomb interaction. In order to avoid all uncertainties connected with an application of the partial wave expansion, unsuitable when working with long-range forces, we apply directly the 3-dimensional pp screened Coulomb t-matrix. That main new ingredient, the 3-dimensional screened pp Coulomb t-matrix, is obtained by a numerical solution of the 3-dimensional Lippmann-Schwinger (LS) equation. Using a simple dynamical model for the nuclear part of the interaction we demonstrate the feasibility of that approach. The physical elastic pd scattering amplitude has a well defined screening limit and does not require renormalisation. Well converged elastic pd cross sections are obtained at finite screening radii. Also the proton-deuteron (pd) breakup observables can be determined from the resulting on-shell 3N amplitudes increasing the screening radius. However, contrary to the pd elastic scattering, the screening limit exists only after renormalisation of the pp t-matrices.

1 Introduction

The inclusion of the Coulomb force into the analysis of nuclear reactions with more than 2 nucleons is a long standing problem. The main reason is the long-range nature of the Coulomb force which prevents the application of the standard techniques developed for short-range interactions. One possible way to avoid the difficulties including the Coulomb force is to use a screened Coulomb interaction and to reach the pure Coulomb limit through application of a renormalisation procedure [1–4].

The problem appears when considering the interaction of protons with deuterons below the pion production threshold. For this 3N system using the Faddeev scheme high-precision numerical predictions for different observables in elastic proton-deuteron (pd) scattering and for the deuteron breakup reaction are being obtained [5], however, only under the restriction to short-ranged nuclear interactions. The high quality of the available pd data for both processes requires, however, in the theoretical analysis the inclusion of the Coulomb force into the calculations. Furthermore the seminal progress [6] in the development of nuclear forces in chiral effective field theory calls also for a very precise solution of the pd scattering equations to test unambiguously these new dynamical ingredients. This test can only be completely satisfactory if the pp Coulomb force is perfectly under control.

For the elastic pd scattering first calculations, with modern nuclear forces and the Coulomb force included, have been achieved in a variational hyperspherical harmonic approach [7]. Only recently the inclusion of the Coulomb force became possible also for the pd breakup reaction [8]. In [8], contrary to [7] where the exact Coulomb force in coordinate representation has been used directly, a screened pp Coulomb force has been applied in momentum space and in a partial wave basis. In order to get the final predictions which can be compared to the data, the limit to the unscreened situation has been performed numerically applying a renormalization to the resulting on-shell amplitudes [8,9]. This allowed for the first time to analyze high-precision pd breakup data and provided a significant improvement of data description in cases where the Coulomb force plays an important role [10].

However, in spite of that substantial progress results of these calculations present concern for two kinematically complete breakup geometries: the pp quasi-free-scattering (QFS) configuration, in which the not detected neutron is at rest in the laboratory system, and the space-star (SST) geometry, in which all 3 outgoing nucleons have the same momenta (magnitudes) in the plane which in the 3N c.m. system is perpendicular to the incoming nucleon momentum. The theoretical predictions based on nuclear forces only show, that the cross sections for QFS and SST are quite stable against changes of the underlying interactions, including also three-nucleon forces [5]. At energies below $\approx$ 20 MeV theory underestimates the SST pd cross sections by $\approx$ 10%, and overestimates the pp QFS cross sections by $\approx$ 20%, respectively [5,8]. With increasing energy the theoretical cross sections come close to the data, which indicates that the pp Coulomb force is very probably re-

[a] e-mail: witala@if.uj.edu.pl

sponsible for these low energy discrepancies. However, the Coulomb force effects found in [8] are practically negligible for the pd SST configuration and only slightly improve the description of the pp QFS data [11–15].

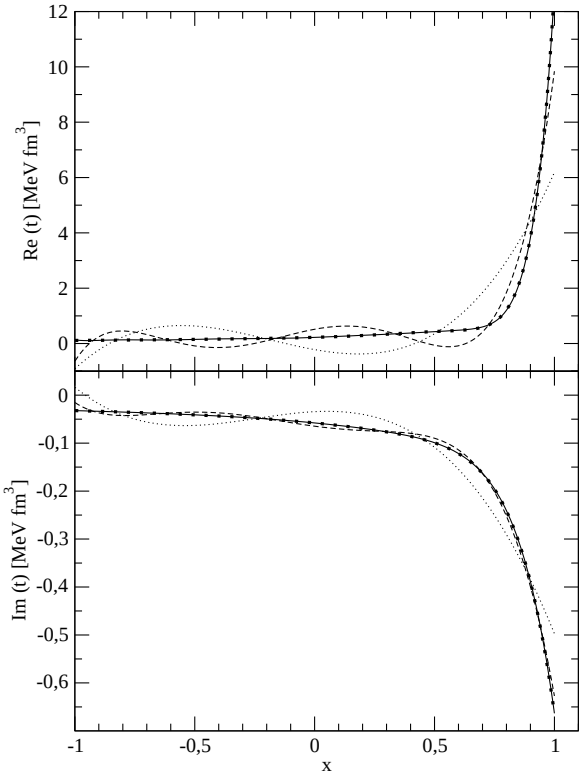

Fig. 1. (color online) The real and imaginary parts of the proton-proton on-shell screened Coulomb t-matrix at $E_p^{lab} = 13$ MeV as a function of the cosine of scattering angle x. The exponential screening with $n = 4$ and screening radius $R = 20$ fm have been used. The full dots represent 3-dimensional screened Coulomb t-matrix obtained by direct solution of the 3-dimensional LS equation. The partial wave summation up to maximal angular momentum $l_{max} = 3$, 5 and 10 are given by dotted, dashed and solid lines, respectively.

This inability to understand the pp QFS and pd SST cross sections calls for reconsidering the inclusion of the Coulomb force into momentum space Faddeev calculations. One main concern in such type of calculations is the application of a partial wave decomposition to the long-ranged Coulomb force. Even when screening is applied it seems reasonable to treat from the beginning the screened pp Coulomb t-matrix without partial wave decomposition because the required limit of vanishing screening leads necessarily to a drastic increase of the number of partial wave states involved. As an example we provide numbers for the exponential screening of the form $e^{-(\frac{r}{R})^n}$. Taking the screening radius $R = 20$ fm and $n = 4$ requires all $l \leq l_{max} = 10$ partial wave states to reproduce the 3-dimensional pp screened Coulomb t-matrix at $E_p^{lab} = 13$ MeV (see Fig.1). Increasing the screening radius to $R = 120$ fm requires at least $l_{max} = 50$ (see Fig.2) which is a big numerical challenge. Even more that would lead to an explosion of the number of 3N partial waves required for convergence.

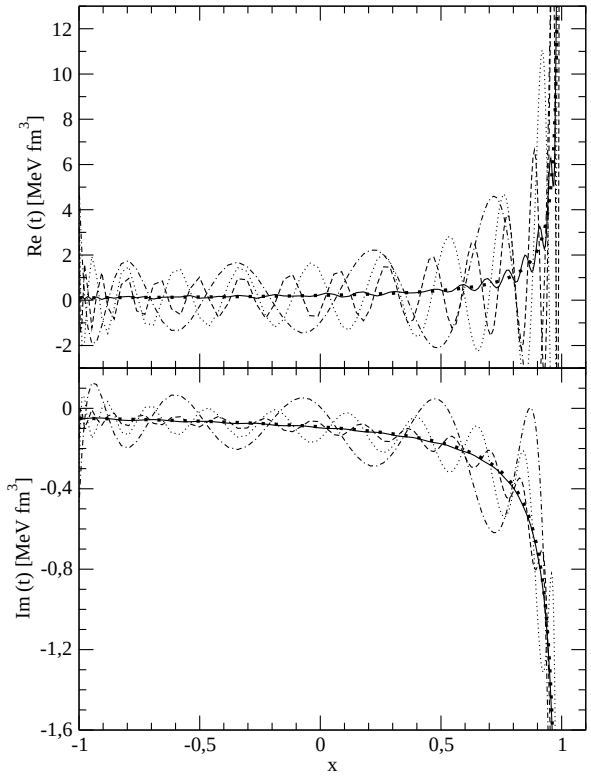

Fig. 2. (color online) The real and imaginary parts of the proton-proton on-shell screened Coulomb t-matrix at $E_p^{lab} = 13$ MeV as a function of the cosine of scattering angle x. The exponential screening with $n = 4$ and screening radius $R = 120$ fm have been used. The full dots represent 3-dimensional screened Coulomb t-matrix obtained by direct solution of the 3-dimensional LS equation. The partial wave summation up to maximal angular momentum $l_{max} = 10$, 20, 30 and 50 are given by dashed-dotted, dotted, dashed and solid lines, respectively.

In [16, 17] we proposed a novel approach to incorporate the pp Coulomb force into the momentum space Faddeev calculations, in which we apply directly the 3-dimensional screened pp Coulomb t-matrix without relying on a partial wave decomposition. 3-dimensional solutions of the LS equation for different screening radii are used to approach the final predictions. We demonstrated, that the physical elastic pd scattering amplitude has a well defined screening limit and does not require renormalisation. In contrast, in case of pp scattering the scattering amplitude requires renormalisation in the screening limit which, however, has not to be applied when only observables have to be addressed [18]. In case of the pd breakup the on-shell solutions of the Faddeev equation are required [17]. They demand renormalisation in the screening limit which can be achieved through renormalisation of the pp t-matrices.

In section 2 we present the main points of the formalism outlined in details in [16, 17]. The pd elastic and breakup transition amplitudes are shown in section 3. The screening limit for pd elastic scattering and breakup is dis-

cussed in section 4 and the results shown in section 5. The summary is given in section 6.

2 Faddeev equations with screened pp Coulomb force

We use the Faddeev equation in the form [5]

$$T|\Phi>=tP|\Phi>+tPG_0T|\Phi> \tag{1}$$

where P is defined in terms of transposition operators, $P = P_{12}P_{23} + P_{13}P_{23}$, G_0 is the free 3N propagator, $|\Phi>$ the initial state composed of a deuteron state and a momentum eigenstate of the proton. Knowing $T|\Phi>$ the breakup as well as the elastic pd scattering amplitudes can be gained by quadratures in the standard manner [5].

We use our standard momentum space partial wave basis $|pq\tilde{\alpha}>$

$$|pq\tilde{\alpha}>\equiv|pq(ls)j(\lambda\frac{1}{2})I(jI)J(t\frac{1}{2})T> \tag{2}$$

and distinguish between the partial wave states $|pq\alpha>$ with total 2N angular momentum j below some value j_{max}: $j \leq j_{max}$, in which the nuclear, V_N, as well as the pp screened Coulomb interaction, V_c^R (in isospin $t = 1$ states only), are acting, and the states $|pq\beta>$ with $j > j_{max}$, for which only V_c^R is acting in the pp subsystem. The states $|pq\alpha>$ and $|pq\beta>$ form a complete system of states

$$\begin{aligned}\mathrm{I} &= \int p^2dpq^2dq\sum_{\tilde{\alpha}}|pq\tilde{\alpha}\rangle\langle pq\tilde{\alpha}| \\ &\equiv \int p^2dpq^2dq(\sum_{\alpha}|pq\alpha\rangle\langle pq\alpha|+\sum_{\beta}|pq\beta\rangle\langle pq\beta|)\end{aligned} \tag{3}$$

Projecting (1) for $T|\Phi>$ on the $|pq\alpha>$ and $|pq\beta>$ states one gets the following system of coupled integral equations

$$\begin{aligned}&\langle pq\alpha|\,T\,|\Phi\rangle = \langle pq\alpha|\,t^R_{N+c}P\,|\Phi\rangle \\ &+\langle pq\alpha|\,t^R_{N+c}PG_0\sum_{\alpha'}\int p'^2dp'q'^2dq'\,\big|p'q'\alpha'\big\rangle \\ &\times\big\langle p'q'\alpha'\big|\,T\,|\Phi\rangle \\ &+\langle pq\alpha|\,t^R_{N+c}PG_0\sum_{\beta'}\int p'^2dp'q'^2dq'\,\big|p'q'\beta'\big\rangle \\ &\times\big\langle p'q'\beta'\big|\,T\,|\Phi\rangle\end{aligned} \tag{4}$$

$$\begin{aligned}&\langle pq\beta|\,T\,|\Phi\rangle = \langle pq\beta|\,t^R_{c}P\,|\Phi\rangle \\ &+\langle pq\beta|\,t^R_{c}PG_0\sum_{\alpha'}\int p'^2dp'q'^2dq'\,\big|p'q'\alpha'\big\rangle \\ &\times\big\langle p'q'\alpha'\big|\,T\,|\Phi\rangle \\ &+\langle pq\beta|\,t^R_{c}PG_0\sum_{\beta'}\int p'^2dp'q'^2dq'\,\big|p'q'\beta'\big\rangle \\ &\times\big\langle p'q'\beta'\big|\,T\,|\Phi\rangle\end{aligned} \tag{5}$$

where t^R_{N+c} and t^R_c are t-matrices generated by the interactions $V_N + V_c^R$ and V_c^R, respectively. Namely for states $|\alpha>$ with two-nucleon subsystem isospin $t = 1$ the corresponding t-matrix element $<p\alpha|t^R_{N+c}(E-\frac{3}{4m}q^2)|p'\alpha'>$ is a linear combination of the pp, t^R_{pp+c}, and the neutron-proton (np), t_{np}, $t = 1$ t-matrices, which are generated by the interactions $V_{pp}^{strong} + V_c^R$ and V_{np}^{strong}, respectively. The coefficients of that combination depend on the total isospin T and T' of states $|\alpha>$ and $|\alpha'>$ [16,19]:

$$\begin{aligned}<t=1T=\frac{1}{2}|t^R_{N+c}|t'=1T'=\frac{1}{2}> &= \frac{1}{3}t_{np}+\frac{2}{3}t^R_{pp+c} \\ <t=1T=\frac{3}{2}|t^R_{N+c}|t'=1T'=\frac{3}{2}> &= \frac{2}{3}t_{np}+\frac{1}{3}t^R_{pp+c} \\ <t=1T=\frac{1}{2}|t^R_{N+c}|t'=1T'=\frac{3}{2}> &= \frac{\sqrt{2}}{3}(t_{np}-t^R_{pp+c}) \\ <t=1T=\frac{3}{2}|t^R_{N+c}|t'=1T'=\frac{1}{2}> &= \frac{\sqrt{2}}{3}(t_{np}-t^R_{pp+c})\end{aligned} \tag{6}$$

For isospin $t = 0$, in which case $T = T' = \frac{1}{2}$:

$$<t=0T=\frac{1}{2}|t^R_{N+c}|t'=0T'=\frac{1}{2}>=t_{np}\,. \tag{7}$$

In case of t_c^R only the screened pp Coulomb force V_c^R is acting.

The third term on the right hand side of (5) is proportional to $<pq\beta|t_c^RPG_0|p'q'\beta'><p'q'\beta'|t_c^R$. A direct calculation of its isospin part shows that independently from the value of the total isospin T it vanishes [16].

Inserting $<pq\beta|T|\Phi>$ from (5) into (4) one gets

$$\begin{aligned}\langle pq\alpha|\,T\,|\Phi\rangle &= \langle pq\alpha|\,t^R_{N+c}P\,|\Phi\rangle+\langle pq\alpha|\,t^R_{N+c}PG_0t^R_cP\,|\Phi\rangle \\ -<pq\alpha|\quad &t^R_{N+c}PG_0\sum_{\alpha'}\int p'^2dp'q'^2dq'\,\big|p'q'\alpha'\big\rangle \\ &\times\langle p'q'\alpha'\big|\,t^R_cP\,|\Phi\rangle \\ &+\langle pq\alpha|\,t^R_{N+c}PG_0\sum_{\alpha'}\int p'^2dp'q'^2dq'\,\big|p'q'\alpha'\big\rangle \\ &\times\langle p'q'\alpha'\big|\,T\,|\Phi\rangle \\ +\langle pq\alpha|\quad &t^R_{N+c}PG_0t^R_cPG_0\sum_{\alpha'}\int p'^2dp'q'^2dq'\,\big|p'q'\alpha'\big\rangle \\ &\times\langle p'q'\alpha'\big|\,T\,|\Phi\rangle \\ &-\langle pq\alpha|\,t^R_{N+c}PG_0\sum_{\alpha'}\int p'^2dp'q'^2dq'\,\big|p'q'\alpha'\big\rangle \\ \times\langle p'q'\alpha'|\quad &t^R_cPG_0\sum_{\alpha''}\int p''^2dp''q''^2dq''\,\big|p''q''\alpha''\big\rangle \\ &\times\langle p''q''\alpha''\big|\,T\,|\Phi\rangle\,.\end{aligned} \tag{8}$$

This is a coupled set of integral equations in the space of the states $|\alpha>$ only, which incorporates the contributions of the pp Coulomb interaction from all partial wave states up to infinity. It can be solved by iteration and Pade summation [5,16].

When compared to our standard treatment without screened Coulomb force [5] there are two new leading terms $<pq\alpha|t^R_{N+c}PG_0t^R_cP|\Phi>$ and $-<pq\alpha|t^R_{N+c}PG_0|\alpha'><\alpha'|t^R_cP|\Phi>$. The first term must be calculated using directly the 3-dimensional screened Coulomb t-matrix t_c^R, while the second term requires partial wave projected screened Coulomb t-matrix elements in the $|\alpha>$ channels only. The kernel also

contains two new terms. The term $< pq\alpha|t^R_{N+c}PG_0t^R_cPG_0|\alpha' >< \alpha'|T|\Phi >$ must again be calculated with a 3-dimensional screened Coulomb t-matrix while the second one, $-< pq\alpha|t^R_{N+c}PG_0|\alpha' >< \alpha'|t^R_cPG_0|\alpha'' >< \alpha''|T|\Phi >$, involves only the partial wave projected screened Coulomb t-matrix elements in the $|\alpha >$ channels. The calculation of the new terms with the partial wave projected Coulomb t-matrices follows our standard procedure. Namely the two sub kernels $t^R_{N+c}PG_0$ and $t^R_cPG_0$ are applied consecutively on the corresponding state. The detailed expressions how to calculate the new terms with the 3-dimensional screened Coulomb t-matrix are given in Appendix A of Ref. [16].

3 The pd elastic and breakup transition amplitudes

The transition amplitude for pd elastic scattering is given by [5,20]

$$\langle \Phi' \big| U \,|\Phi\rangle = \langle \Phi' \big| PG_0^{-1} + PT \,|\Phi\rangle \ . \tag{9}$$

That amplitude has two contributions. The first one is independent of the pp Coulomb force [16]

$$< \Phi'|PG_0^{-1}|\Phi >=< \Phi'|PV|\Phi >= -\frac{1}{2} < \phi'|P_{00}V^{00}_{np}|\phi > \tag{10}$$

where P_{00} acts only in spin-momentum space

$$P_{tt'} = P_{12}P_{23} + (-)^{t+t'}P_{13}P_{23}|_{spin-momentum} \ . \tag{11}$$

To calculate the second part of the matrix element (9) one needs $\langle \mathbf{pq} \,|\, T \,|\Phi\rangle$ composed of low and high partial wave contributions for $T|\Phi >$. It enters also the transition amplitude for breakup $< \Phi_0|U_0|\Phi >$ which is given in terms of $T\,|\Phi\rangle$ by [5,20]

$$\langle \Phi_0| \, U_0 \,|\Phi\rangle = \langle \Phi_0| \, (1+P)T \,|\Phi\rangle \tag{12}$$

where $|\Phi_0 >= |\mathbf{pq}m_i\nu_i >$ $(i = 1,2,3)$ is the free state. The permutations acting in momentum-, spin-, and isospin-spaces can be applied to the bra-state $< \phi_0| =< \mathbf{pq}m_i\nu_i|$ changing the sequence of nucleons spin and isospin magnetic quantum numbers m_i and ν_i and leading to well known linear combinations of the Jacobi momenta $\mathbf{p}, \mathbf{q}$. Thus evaluating (12) it is sufficient to regard the general amplitudes $< \mathbf{pq}m_1m_2m_3\nu_1\nu_2\nu_3|T\,|\Phi\rangle \equiv \langle \mathbf{pq} \,|\, T \,|\Phi\rangle$. Using Eq. (1) and the completness relation (3) one gets:

$$\begin{aligned}
&\langle \mathbf{pq} \,|\, T \,|\Phi\rangle = \langle \mathbf{pq} \,|\, \sum_{\alpha'} \int p'^2dp'q'^2dq' \,\big|p'q'\alpha'\big\rangle \\
&\times \big\langle p'q'\alpha' \big| \, T \,|\Phi\rangle \\
&\quad - \langle \mathbf{pq} \,|\, \sum_{\alpha'} \int p'^2dp'q'^2dq' \,\big|p'q'\alpha'\big\rangle \\
&\times \big\langle p'q'\alpha' \big| \, t^R_cP \,|\Phi\rangle \\
&\quad - \langle \mathbf{pq} \,|\, \sum_{\alpha'} \int p'^2dp'q'^2dq' \,\big|p'q'\alpha'\big\rangle \\
&\times \big\langle p'q'\alpha' \big| \, t^R_cPG_0 \sum_{\alpha''} \int p''^2dp''q''^2dq'' \,\big|p''q''\alpha''\big\rangle \\
&\times \big\langle p''q''\alpha'' \big| \, T \,|\Phi\rangle \\
&\quad + \langle \mathbf{pq} \,|\, t^R_cP \,|\Phi\rangle \\
&\quad + \langle \mathbf{pq} \,|\, t^R_cPG_0 \sum_{\alpha'} \int p'^2dp'q'^2dq' \,\big|p'q'\alpha'\big\rangle \\
&\times \big\langle p'q'\alpha' \big| \, T \,|\Phi\rangle \ .
\end{aligned} \tag{13}$$

It follows, that in addition to the Faddeev amplitudes $< pq\alpha|T|\Phi >$ also the partial wave projected amplitudes $< pq\alpha|t^R_cP|\Phi >$ and $< pq\alpha|t^R_cPG_0|\alpha' >< \alpha'|T|\Phi >$ are required. The expressions for the contributions of these three terms to the transition amplitude for elastic scattering and breakup reaction are given in Appendix B of Ref. [16].

The last two terms in (13) again must be calculated using directly 3-dimensional screened Coulomb t-matrices. In Appendix C of Ref. [16] the expression for $\langle \mathbf{pq} \,|\, t^R_cP \,|\Phi\rangle$ and in Appendix D of Ref. [16] the last matrix element $< \mathbf{pq} \,|t^R_cPG_0|\alpha' >< \alpha'|T|\Phi >$ are given.

4 The screening limit

The set of coupled Faddeev equations (8) is well defined for a finite screening radius. It is an exact set assuming that the strong NN t-matrix can be neglected beyond a certain j_{max}, which is justified. Further the pp screened Coulomb force is taken into account to infinite order in the partial wave decomposition in form of the 3-dimensional screened Coulomb t-matrix t^{cR}_{pp}. The important challenge is to control the screening limit for the physical pd elastic scattering amplitude (9) and for the physical pd breakup amplitude (12).

For the pd elastic scattering the contribution (10) is well defined and independent of the Coulomb force. The corresponding expression without partial-wave expansion is given in Appendix C (C.5) of [16]. In [16] analytical arguments were provided that also other terms contributing to the elastic scattering amplitude has a well defined screening limit and does not require renormalisation. Thus also the physical on-shell elastic pd amplitude has a well defined screening limit and does not require renormalisation. This can be traced back to the fact that to get the elastic pd scattering amplitude it is sufficients to solve the Faddeev equations (8) for off-shell values of the Jacobi momenta

$$\frac{p^2}{m} + \frac{3}{4m}q^2 \neq E \ . \tag{14}$$

The off-shell Faddeev amplitudes $\langle pq\alpha| \, T \,|\Phi\rangle$ of Eq.(8) are determined by off-shell nucleon-nucleon t-matrix elements $t(p,p';E-\frac{3}{4m}q^2)$, which have a well defined screening limit (see the following discussion and examples).

The case of the pd breakup process is quite different. Contrary to pd elastic scattering the physical breakup amplitude (12) corresponds to the on-shell values of Jacobi momenta

$$\frac{p^2}{m} + \frac{3}{4m}q^2 = E \equiv \frac{3}{4m}q^2_{max} \ . \tag{15}$$

That means that the physical pd breakup amplitude (12) requires on-shell Faddeev amplitudes $\langle p_0q\alpha| \, T \,|\Phi\rangle$ together

with the four, also on-shell, additional terms in (13), with $p_0 = \sqrt{\frac{3}{4}(q_{max}^2 - q^2)}$. The on-shell Faddeev amplitudes can be obtained from the off-shell solutions $\langle pq\alpha|\, T\,|\Phi\rangle$ using (8):

$$\begin{aligned}
&\langle p_0 q\alpha|\, T\,|\Phi\rangle = \langle p_0 q\alpha|\, t^R_{N+c} P\,|\Phi\rangle \\
&+ \langle p_0 q\alpha|\, t^R_{N+c} P G_0 t^R_c P\,|\Phi\rangle \\
&- \langle p_0 q\alpha|\, t^R_{N+c} P G_0 \sum_{\alpha'} \int p'^2 dp' q'^2 dq' \,\big|p' q' \alpha'\big\rangle \\
&\times \big\langle p' q' \alpha'\big|\, t^R_c P\,|\Phi\rangle \\
&+ \langle p_0 q\alpha|\, t^R_{N+c} P G_0 \sum_{\alpha'} \int p'^2 dp' q'^2 dq' \,\big|p' q' \alpha'\big\rangle \\
&\times \big\langle p' q' \alpha'\big|\, T\,|\Phi\rangle \\
&+ \langle p_0 q\alpha|\, t^R_{N+c} P G_0 t^R_c P G_0 \sum_{\alpha'} \int p'^2 dp' q'^2 dq' \,\big|p' q' \alpha'\big\rangle \\
&\times \big\langle p' q' \alpha'\big|\, T\,|\Phi\rangle \\
&- \langle p_0 q\alpha|\, t^R_{N+c} P G_0 \sum_{\alpha'} \int p'^2 dp' q'^2 dq' \,\big|p' q' \alpha'\big\rangle \\
&\times \big\langle p' q' \alpha'\big|\, t^R_c P G_0 \sum_{\alpha''} \int p''^2 dp'' q''^2 dq'' \,\big|p'' q'' \alpha''\big\rangle \\
&\times \big\langle p'' q'' \alpha''\big|\, T\,|\Phi\rangle \ . \qquad (16)
\end{aligned}$$

These on-shell amplitudes together with additional, also on-shell, terms in (13) define the physical breakup amplitude (12). That in consequence requires half-shell t-matrix elements $t(p_0, p'; \frac{p_0^2}{m})$ which are of 3 types: the partial wave projected pure screened Coulomb t^R_c generated by V^R_c, the partial wave projected t^R_{N+c} generated by $V_{strong} + V^R_c$, and the 3-dimensional screened Coulomb matrix elements.

It is well known [1,21,22] that in the screening limit $R \to \infty$ such half-shell t-matrices acquire an infinitely oscillating phase factor $e^{i\Phi_R(p)}$, where $\Phi_R(p)$ depends on the type of the screening. For the exponential screening used in the present study its form depends on two parameters, the screening radius R and the power n:

$$V^R_c(r) = \frac{\alpha}{r} e^{-(\frac{r}{R})^n} \ . \qquad (17)$$

At a given value n the pure Coulomb potential results for $R \to \infty$. As has been shown in [23] based on [24,25], the related phase $\Phi_R(p)$ is given as

$$\Phi_R(p) = -\eta[ln(2pR) - \epsilon/n] \qquad (18)$$

where $\epsilon = 0.5772\ldots$ is the Euler number and $\eta = \frac{m_p \alpha}{2p}$ the Sommerfeld parameter.

Contrary to the half-shell, the off-shell t-matrix elements do not acquire such an oscillating phase and their screening limit is well defined.

In Figs. 3-4 we demonstrate that behavior for the 3-dimensional half-shell screened Coulomb pp t-matrix [18]. Increasing the screening radius R changes drastically the imaginary part of the t-matrix (Fig. 4a). The real part is more stable but does not approach the pure Coulomb limit (Fig. 3a). Renormalizing by the phase factor $e^{-i\Phi_R(p)}$ of Eq. (18) provides a well defined limit to the pure Coulomb half-shell result of Ref. [26] (Fig. 3b and 4b).

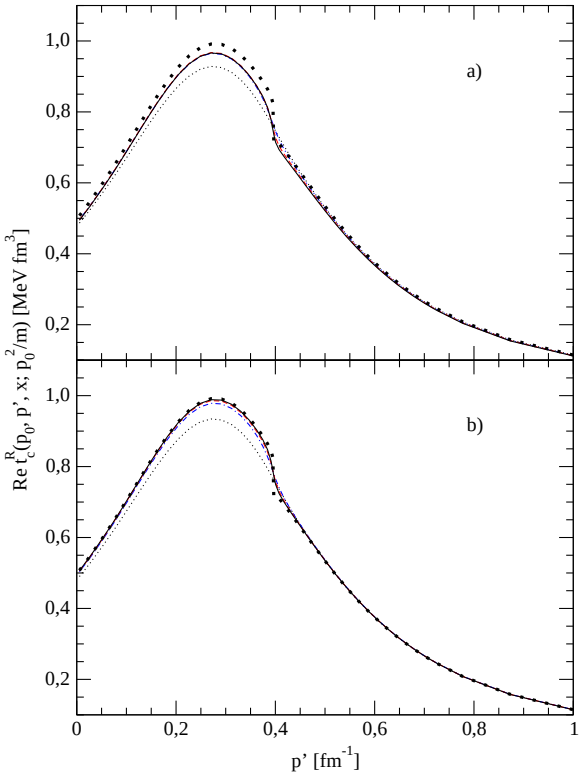

Fig. 3. (color online) The real part of the nonrenormalized (a) and renormalized (b) 3-dimensional half-shell screened Coulomb pp t-matrix $t^R_c(p_0, p', x; \frac{p_0^2}{m})$. The lines correspond to the exponential screening with $n = 1$ and different screening radia: $R = 20$ fm (black dotted line), $R = 60$ fm (blue dashed-dotted line), $R = 120$ fm (red dashed line), $R = 180$ fm (black solid line). The Coulomb half-shell result of Ref. [26] is given by thick dots. The momentum $p_0 = 0.396$ fm^{-1} and $x = 0.706$.

For the 3-dimensional off-shell screened Coulomb pp t-matrix the pure Coulomb screening limit of Ref. [28,27] is achieved without any renormalisation factor for screening radia $R > 20$ fm (Fig. 5).

Analogous behavior for the partial wave decomposed $l = 0$ half-shell screened Coulomb t^R_c and the $^1S_0$ t^R_{pp+c} t-matrices is shown in Figs. 6 and 7, respectively. While the imaginary part again exhibits drastic changes when the screening radius increases (Fig. 6a and 7a), removing the phase factor $e^{-i\Phi_R(p)}$ (renormalisation) provides a well defined limit for the screening radia $R > 40$ fm (Fig. 6b and 7b). It is seen that in case when the screened Coulomb potential is combined with the strong force also the real part of the half-shell t-matrix undergoes strong changes with increased screening (Fig. 7a).

For the partial wave decomposed off-shell $l = 0$ screened Coulomb t^R_c and the $^1S_0$ t^R_{pp+c} t-matrix elements a well defined screening limit is reached without any renormalisation (Fig. 8b and 8a, respectively).

That oscillatory phase factor appearing in the half-shell proton-proton t-matrices requires a carefull treatment of (16) to get the screening limit for the $\langle p_0 q\alpha|\, T\,|\Phi\rangle$ amplitudes. Namely for the states $|\alpha >$ with the two-nucleon subsystem isospin $t = 1$ the corresponding t-matrix element

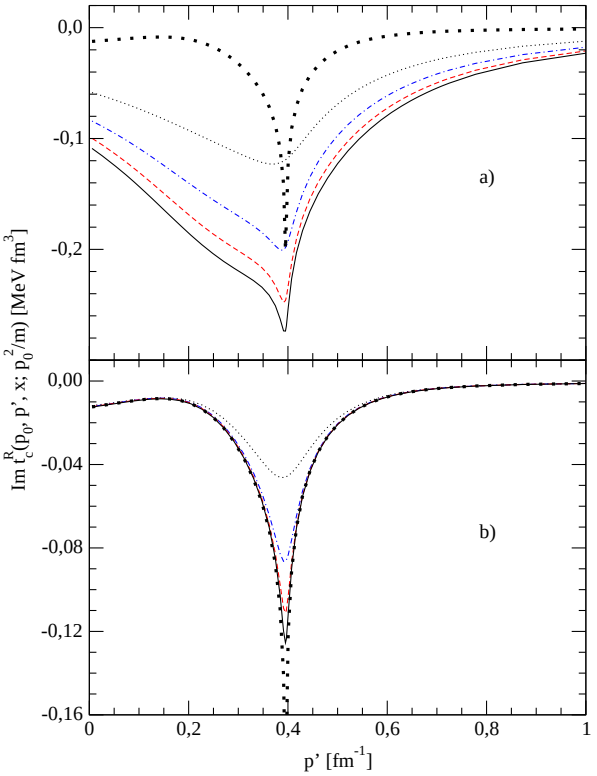

Fig. 4. (color online) The imaginary part of the nonrenormalized (a) and renormalized (b) 3-dimensional half-shell screened Coulomb pp t-matrix $t_c^R(p_0, p', x; \frac{p_0^2}{m})$. For the description of the lines and values of p_0 and x see Fig. 3.

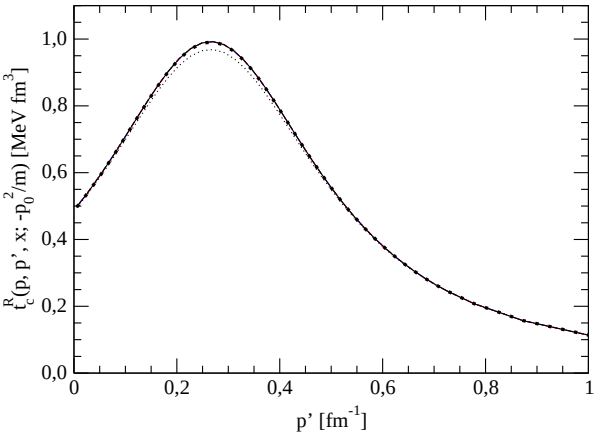

Fig. 5. (color online) The 3-dimensional off-shell screened Coulomb pp t-matrix $t_c^R(p, p', x; -\frac{p_0^2}{m})$. The lines correspond to the exponential screening with $n = 1$ and different screening radia: $R = 20$ fm (black dotted line), $R = 60$ fm (blue dashed-dotted line), $R = 120$ fm (red dashed line), $R = 180$ fm (black solid line). The Coulomb off-shell result of Ref. [28,27] is given by thick dots. The momentum $p_0 = 0.396$ fm^{-1}, $p = 0.375$ fm^{-1} and $x = 0.706$.

$< p_0\alpha|t_{N+c}^R(\frac{p_0^2}{m})|p'\alpha' >$ is a linear combination of the pp and neutron-proton (np) $t = 1$ t-matrices, the coefficients of which depend on the total isospin T and T' of the states $|\alpha >$ and $|\alpha' >$ (see discussion after (5)). It follows that

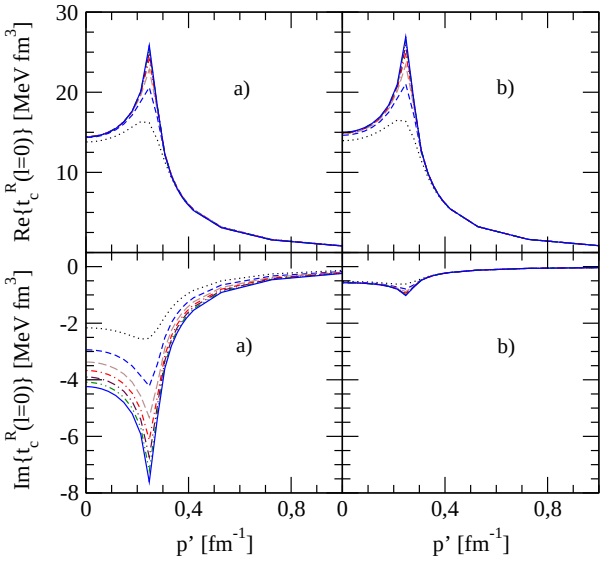

Fig. 6. (color online) The real (upper panels) and imaginary (lower panels) parts of the nonrenormalized (a) and renormalized (b) $l = 0$ half-shell screened Coulomb pp t-matrix $t_c^R(p_0, p', \frac{p_0^2}{m})$. The lines correspond to the exponential screening with $n = 1$ and different screening radia: $R = 20$ fm (black dotted line), $R = 40$ fm (blue short-dashed line), $R = 60$ fm (brown long-dashed line), $R = 80$ fm (red short-dashed-dotted line), $R = 100$ fm (maroon long-dashed-dotted line), $R = 120$ fm (green short-dashed-double-dotted line), $R = 140$ fm (blue solid line). The momentum $p_0 = 0.26$ fm^{-1}.

to achieve the screening limit one needs to renormalize the pp t-matrix t_{pp+c}^R in that combination before performing the action of the operators in (16). The term in that linear combination coming with the np t-matrix t_{np} does not require renormalisation.

5 Numerical results

To demonstrate the feasibility of our approach we applied the outlined formalism to a simple dynamical model in which the nucleon-nucleon force was restricted to act in ${}^1S_0$ and ${}^3S_1 - {}^3D_1$ partial waves only and taken from the CD Bonn potential [29]. The proton-proton Coulomb force was modified by the exponential screening (17) with the screening radius R and $n = 1$.

To investigate the screening limit $R \to \infty$ we generated set of partial-wave decomposed t-matrices, t_c^R, based on the screened pp Coulomb force only or combined with the strong pp interaction, t_{pp+c}^R, taking $R = 20, 40, 60, 80, 100,$ 120 and 140 fm. With that dynamical input we solved the set of Faddeev equations (8) for off-shell values of the Jacobi momenta p and q and for the total angular momenta of the p-p-n system up to $J \leq \frac{15}{2}$ and both parities. Then the on-shell Faddeev amplitudes $\langle p_0 q\alpha|\, T\, |\Phi\rangle$ were gained through (16). In this first study we restricted ourselves to the perturbative approximation for the 3-dimensional screened Coulomb t-matrix: $t_c^R = V_c^R$. In the future studies that approximation will be avoided and the full solution of the

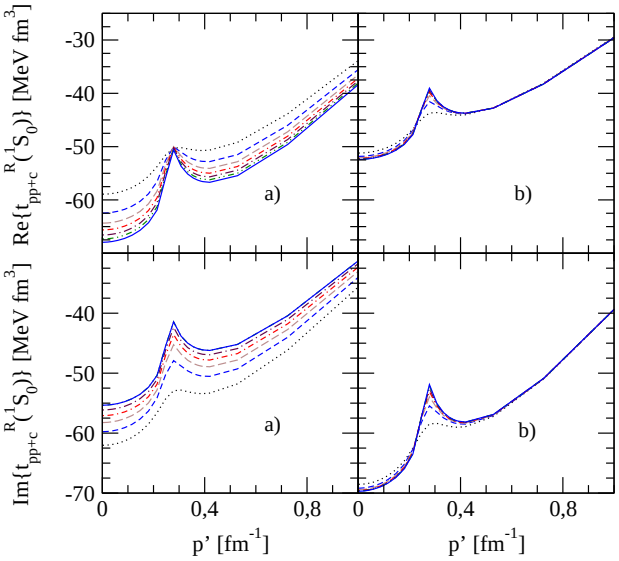

Fig. 7. (color online) The real (upper panels) and imaginary (lower panels) parts of the nonrenormalized (a) and renormalized (b) $^1S_0$ half-shell pp t-matrix $t^R_{pp+c}(p_0, p', \frac{p_0^2}{m})$. The lines correspond to the exponential screening with $n = 1$ and different screening radia: $R = 20$ fm (black dotted line), $R = 40$ fm (blue short-dashed line), $R = 60$ fm (brown long-dashed line), $R = 80$ fm (red short-dashed-dotted line), $R = 100$ fm (maroon long-dashed-dotted line), $R = 120$ fm (green short-dashed-double-dotted line), $R = 140$ fm (blue solid line). The momentum $p_0 = 0.26$ fm^{-1}.

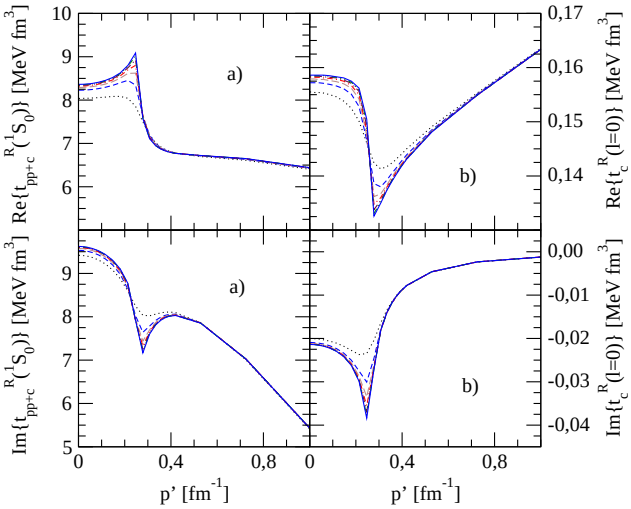

Fig. 8. (color online) The real (upper panels) and imaginary (lower panels) parts of the $^1S_0$ $t^R_{pp+c}(p, p', \frac{p_0^2}{m})$ (a) and the $l = 0$ screened Coulomb $t^R_c(p, p', \frac{p_0^2}{m})$ (b) off-shell t-matrices. For the description of the lines see Fig. 6. The momentum $p_0 = 0.26$ fm^{-1} and $p = 2.38$ fm^{-1}.

3-dimensional LS equation for the screened pp Coulomb t-matrix will be used [18]. When calculating observables we also omitted the last term in (13) coming with the 3-dimensional screened Coulomb t-matrix, $\langle \mathbf{pq}|t^R_c PG_0 T|\Phi\rangle$.

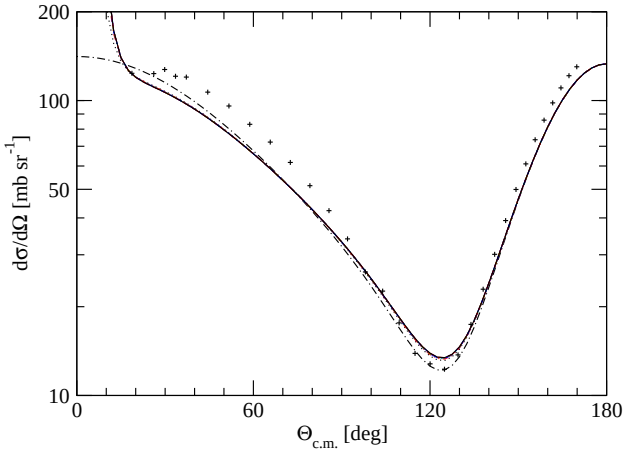

Fig. 9. (color online) The convergence in the cut-off radius R of the pd elastic scattering cross section $\frac{d\sigma}{d\Omega}$ shown as a function of the c.m. angle $\Theta_{c.m.}$ at the incoming proton energy $E_p^{lab} = 13$ MeV. These cross sections were calculated with the screened Coulomb force and the CD Bonn nucleon-nucleon potential [29] restricted to the $^1S_0$ and $^3S_1$-$^3D_1$ partial waves. The screening radii are : $R = 20$ fm (black dotted line), $R = 40$ fm (green double-dashed - dotted line), $R = 60$ fm (blue long-dashed-dotted line), $R = 80$ fm (red dashed- double-dotted line), $R = 100$ fm (blue short-dashed line), $R = 120$ fm (red long-dashed line), $R = 140$ fm (black solid line). The $R = 40$-140 fm lines are practically overlapping. The black dashed-dotted line is the corresponding nd elastic scattering cross section. The pluses are $E_p^{lab} = 12$ MeV pd elastic scattering cross section data of Ref. [30].

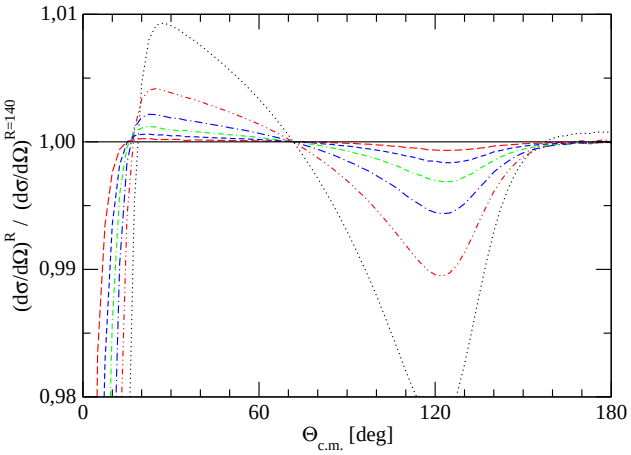

Fig. 10. (color online) The convergence in the cut-off radius R of the pd elastic scattering cross section $\frac{d\sigma}{d\Omega}$ at the incoming proton energy $E_p^{lab} = 13$ MeV, shown as the ratio $\frac{d\sigma}{d\Omega}^R / \frac{d\sigma}{d\Omega}^{R=140}$. For the description of the lines see Fig. 9.

In Fig. 9 we show the convergence in the screening radius R of the pd elastic scattering cross section and compare the pd and nd elastic scattering angular distributions at the incoming nucleon energy $E_N^{lab} = 13$ MeV. On the scale of the figure the cross sections for $R = 40 - 140$ fm are practically indistinguishable. The detailed picture of that convergence is depicted in Fig. 10, where the ratio of the cross sections obtained with the screening radius R to those with $R = 140$ fm is shown as a function of the c.m.

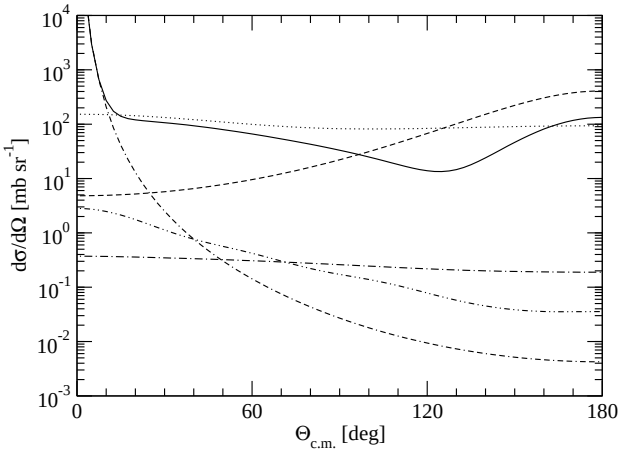

Fig. 11. The contributions of different terms to the pd elastic scattering cross section $\frac{d\sigma}{d\Omega}$ at the incoming proton energy $E_p^{lab} = 13$ MeV calculated with the screening radius $R = 100$ fm. The dotted and dashed lines are contributions of the $\langle \Phi' | PT | \Phi \rangle$ and $\left\langle \Phi' | PG_0^{-1} | \Phi \right\rangle$ terms, respectively. The double-dashed-dotted line is the contribution of the $\left\langle \Phi' | Pt_c^R P | \Phi \right\rangle$ term coming with the 3-dimensional screened Coulomb t-matrix t_c^R. The dashed-double-dotted and dashed-dotted lines are contributions of the $\left\langle \Phi' | Pt_c^R P | \Phi \right\rangle$ and $\left\langle \Phi' | Pt_c^R PG_0 T | \Phi \right\rangle$ terms, respectively, which are calculated with the partial-wave decomposed screened Coulomb t-matrix. The solid line encompasses all terms. In this feasibility study the 3-dimensional t_c^R is replaced by V_c^R.

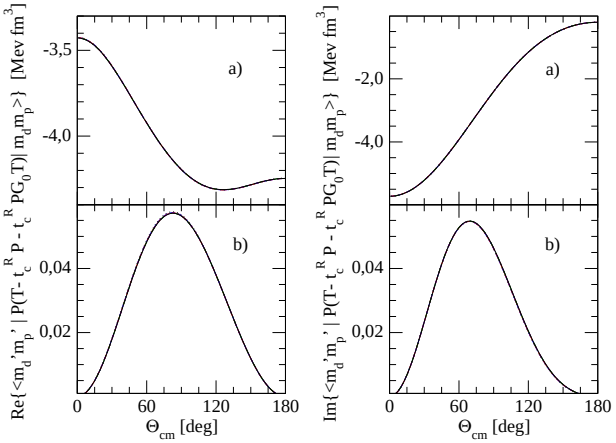

Fig. 12. (color online) The independence of the real (left column) and imaginary (right column) parts of the partial wave contribution $\left\langle \Phi'_{m_{d'} m_{p'}} | P(T - t_c^R P - t_c^R PG_0 T) | \Phi_{m_d m_p} \right\rangle$ to the $E_p^{lab} = 13$ MeV pd elastic scattering transition amplitude on the cut-off radius R. The different lines are: $R = 20$ fm - dotted, $R = 40$ fm - short-dashed, $R = 60$ fm - long-dashed, $R = 80$ fm - short-dashed-dotted, $R = 100$ fm - long-dashed-dotted, $R = 120$ fm - double-dotted-dashed, $R = 140$ fm - solid. All the lines are practically overlapping. The incoming and outgoing deuteron and proton spin projections are for a): $m_d = m_{d'} = -1$ and $m_p = m_{p'} = -\frac{1}{2}$ and for b): $m_d = -1$, $m_{d'} = +1$, and $m_p = m_{p'} = +\frac{1}{2}$.

scattering angle $\Theta_{c.m.}$. It is clearly seen that already with the screening radius $R = 40$ fm converged results for the cross section are achieved. Increasing further the value of R provides cross sections which differ less than $\approx 1\%$ up to the forward scattering angles $\Theta_{c.m.} \approx 10^o$. At very forward angles, where the pp Coulomb force is dominant, larger screening radii are required to get the cross section with the same precision.

The angular distributions shown in Figs. 9 and 10 were obtained taking in the elastic scattering transition amplitude (9) the exchange term $\left\langle \Phi' | PG_0^{-1} | \Phi \right\rangle$ together with the first four terms in (13) contributing to $\langle \Phi' | PT | \Phi \rangle$. In Fig. 11 we present how each term contributes to the cross section. When all terms are taken into account the resulting angular distribution is given by the solid line. The $< \Phi' | PT | \Phi >$ term (dotted line related to the first term in (13)) contributes significantly at all angles. At backward angles the largest contribution comes from the exchange term $< \Phi' | P G_0^{-1} | \Phi >$ (dashed line) while at forward angles the most important is the "Rutherford" term $\left\langle \Phi' | Pt_c^R P | \Phi \right\rangle$ (double-dashed-dotted line related to the fourth term in (13)) calculated with the 3-dimensional screened Coulomb t-matrix t_c^R (in this first study treated perturbatively as $t_c^R = V_c^R$). The two terms based on the partial-wave projected Coulomb t-matrix, $< \Phi' | Pt_c^R P | \Phi >$ (dashed-double-dotted line related to the second term in (13)) and $\left\langle \Phi' | Pt_c^R PG_0 T | \Phi \right\rangle$ (dashed-dotted line related to the third term in (13)), are about 2-orders of magnitude smaller and thus of minor importance. The fact that at very forward angles the contribution of the $< \Phi' | Pt_c^R PG_0 T | \Phi >$ is an order of magnitude smaller than the contribution of the $\left\langle \Phi' | Pt_c^R P | \Phi \right\rangle$ seems to justify the neglection of the last term $\left\langle \Phi' | Pt_c^R PG_0 T | \Phi \right\rangle$ in (13) coming with the 3-dimensional screened Coulomb t-matrix. In future studies this term will be calculated to verify this statement.

In Fig. 12 we demonstrate numerically that the elastic pd amplitude has a well defined screening limit and does not require renormalization. The real and imaginary parts of the partial wave contribution $< \Phi' | P(T + t_c^R P + t_c^R PG_0 T) | \Phi >$ to the elastic transition amplitude are shown for two combinations of the incoming and outgoing deuteron and proton spin projections and a number of screening radia $R = 20, 40, 60, 80, 100, 120$, and 140 fm. The additional term (10) is real and independent of the screening radius. The fourth term in (13) is also real under our approximation $t_c^R = V_c^R$ and for angles different from zero has a well defined screening limit. Moreover it is peaked in forward direction and would dominate terms shown. All lines are practically overlapping. That shows that not only the cross section but the pd elastic scattering amplitude itself does not develop an oscillating phase in the infinite screening limit.

The results for the breakup reaction are shown in Figs. 13 - 16 where the exclusive cross sections $\frac{d^5\sigma}{d\Omega_1 \Omega_2 dS}$ for the QFS and SST configurations parametrized through the arc-length of the kinematical S-curve are presented.

For the QFS and SST (see Fig. 13 and 15, respectively) the convergence in the screening radius is achieved at $R =$ 60 fm. For QFS the Coulomb force decreases the cross section with respect to the nd case and brings the theory close to the pd data. For SST the Coulomb force also brings the-

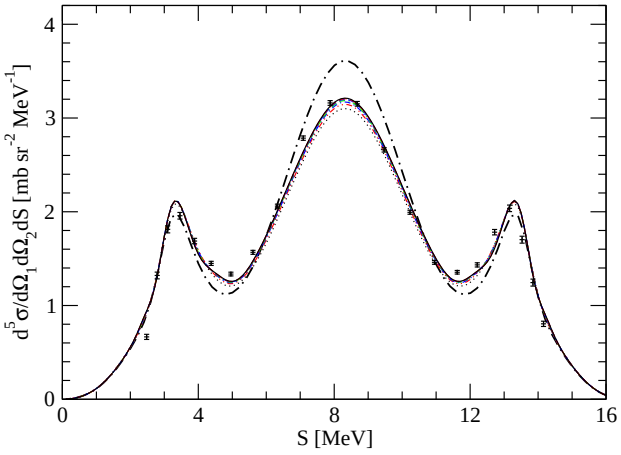

Fig. 13. (color online) The convergence in the cut-off radius R of the $d(p, p_1p_2)n$ breakup cross section in a kinematically complete QFS configuration with polar angles of the two outgoing protons $\theta_1 = \theta_2 = 39^o$ and azimuthal angle $\phi_{12} = 180^o$. The incoming proton energy is $E_p^{lab} = 13$ MeV and theoretical predictions are based on a screened Coulomb force and the CD Bonn nucleon-nucleon potential [29] restricted to $^1S_0$ and $^3S_1$-$^3D_1$ partial waves. The screening radius is: $R = 20$ fm (black dotted line), $R = 40$ fm (green dashed-double-dotted line), $R = 60$ fm (blue dashed-dotted line), $R = 80$ fm (red double-dashed-dotted line), $R = 100$ fm (blue dashed line), $R = 120$ fm (red long-dashed line), $R = 140$ fm (black solid line). The black long-dashed-dotted line is the break-up cross section with the pp Coulomb interaction switched-off. The pluses are $E_p^{lab} = 13$ MeV pd breakup data of Ref. [11].

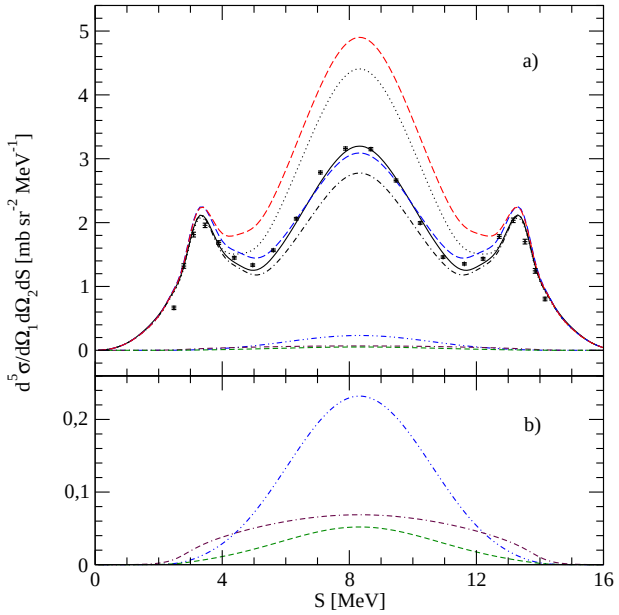

Fig. 14. (color online) In part a): the contribution of different terms to the cross section of the QFS configuration of Fig. 13. The (black) dashed-dotted line is the contribution of the first term $\langle\Phi_0|(1+P)|\alpha><\alpha|T|\Phi\rangle$ in (13) and the (green) short-dashed line is the contribution of the fourth term $\left\langle\Phi_0|(1+P)t_c^RP|\Phi\right\rangle$ in (13) coming with the 3-dimensional screened Coulomb t-matrix t_c^R (in the present calculation $t_c^R = V_c^R$). The (blue) dashed-double-dotted and (maroon) double-dashed-dotted lines are contributions of the second $\left\langle\Phi_0|(1+P)|\alpha><\alpha|t_c^RP|\Phi\right\rangle$ and of the third $\left\langle\Phi_0|(1+P)|\alpha><\alpha|t_c^RPG_0T|\Phi\right\rangle$ term in (13), respectively, which are calculated with partial-wave decomposed screened Coulomb t-matrix. The (black) dotted and (blue) long-dashed lines result from the $\left\langle\Phi_0|(1+P)|\alpha><\alpha|(T-t_c^RP)|\Phi\right\rangle$ and $\left\langle\Phi_0|(1+P)|\alpha><\alpha|(T-t_c^RPG_0T)|\Phi\right\rangle$ amplitudes, respectively. The (red) long-dashed line is the contribution of the $\left\langle\Phi_0|(1+P)|\alpha><\alpha|(T-t_c^RP-t_c^RPG_0T)|\Phi\right\rangle$ amplitude. The (black) solid line encompasses all four terms. All results are for screening radius $R = 100$ fm. The part b) of the figure shows contributions of small terms which are difficult to see on the scale of part a).

ory close to the pd data, however, only at S-values close to the space-star condition ($S \approx 6$ MeV). For S-values further away the theory is far above the pd data.

The theoretical prediction for both geometries results through interference of different terms contributing to the breakup amplitude. The importance and magnitudes of the contributions coming from different terms in the breakup amplitude differs for those two geometries (see Fig. 14 and Fig. 16). In both cases the largest is the contribution of the first term in (13) $<\Phi_0|(1+P)|\alpha><\alpha|T|\Phi>$ (black dashed-dotted line in Figs. 14 and 16). For QFS and SST the cross section resulting from that term is below the pd data and below the full result which encompasses all terms (solid line). The magnitudes of three additional terms: $<\Phi_0|(1+P)\,t_c^RP|\Phi>$ (the fourth term in (13) calculated with the 3-dimensional screened Coulomb t-matrix, here approximated by V_c^R, and given by the green short-dashed line), the second term in (13) $\left\langle\Phi_0|(1+P)|\alpha><\alpha|t_c^RP|\Phi\right\rangle$ (calculated with the partial-wave projected screened Coulomb t-matrix and given by the blue dashed-double-dotted line), and the third term in (13) $<\Phi_0|(1+P)|\alpha><\alpha|t_c^RPG_0T|\Phi>$ (calculated again with the partial-wave projected screened Coulomb t-matrix and given by the maroon double-dashed-dotted line), are small. Because they are difficult to see on the scale of Figs. 14a and Fig. 16a they are again presented in the part b) of these figures. For both configurations the term with the 3-dimensional t-matrix $<\Phi_0|(1+P)\,t_c^RP|\Phi>$ gives the smallest contribution. Smallness of these terms does not mean however, that they are unimportant because the interference effects are nonnegligible and act in different ways for QFS and SST.

For the QFS the second largest contribution comes from $\left\langle\Phi_0|(1+P)|\alpha><\alpha|t_c^RP|\Phi\right\rangle$ (blue dashed-double-dotted line) while for SST it comes from $<\Phi_0|(1+P)|\alpha><\alpha|t_c^RPG_0T|\Phi>$ (maroon double-dashed-dotted line). For QFS and SST taking the amplitude of that second largest contribution together with $\langle\Phi_0|(1+P)|\alpha><\alpha|T|\Phi\rangle$ changes significantly the cross section. For QFS it is the black dotted line in Fig. 14a resulting from $<\Phi_0|(1+P)|\alpha><\alpha|(T-t_c^RP)|\Phi>$ while for SST it is blue long-dashed line in Fig. 16a resulting from $<\Phi_0|(1+P)|\alpha><\alpha|(T-t_c^RPG_0T)|\Phi>$.

The third largest contribution provides for both configurations smaller changes of the cross section and the result when the second and third largest contributions are in-

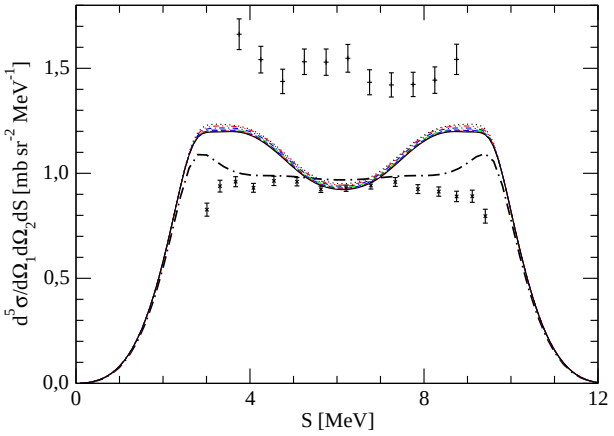

Fig. 15. (color online) The convergence in the cut-off radius R of the $d(p, p_1p_2)n$ breakup cross section in a kinematically complete SST configuration with polar angles of the two outgoing protons $\theta_1 = \theta_2 = 50.5^o$ and azimuthal angle $\phi_{12} = 120^o$. The incoming proton energy is $E_p^{lab} = 13$ MeV and the theoretical predictions are based on the screened Coulomb force and the CD Bonn nucleon-nucleon potential [29] restricted to $^1S_0$ and $^3S_1$-$^3D_1$ partial waves. For the description of the lines see Fig. 13. The x-es are $E_p^{lab} = 13$ MeV pd breakup data of Ref. [11] and pluses are $E_n^{lab} = 13$ MeV nd breakup data of Ref. [31].

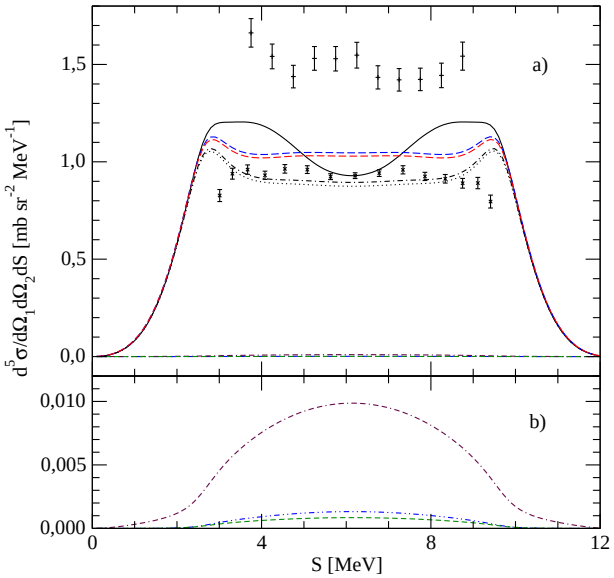

Fig. 16. (color online) In part a): the contribution of different terms to the cross section of the SST configuration of Fig. 15. The solid line encompasses all terms. For the description of other lines see Fig. 14. All results are for screening radius $R = 100$ fm. The part b) of the figure shows contributions of small terms which are difficult to see on the scale of part a).

cluded $\left\langle \Phi_0|(1+P)|\alpha><\alpha|(T - t_c^R P G_0 T - t_c^R P)|\Phi\right\rangle$ is given by the red long-dashed line. It is above the pd data for both geometries.

Finally, including the smallest contribution from the 3-dimensional screened Coulomb t-matrix $\left\langle \Phi_0|(1+P)t_c^R P|\Phi\right\rangle$ brings the theory to the pd data for the QFS geometry at all S-values and for the SST configuration at S-values close to the space-star condition.

6 Summary and conclusions

We presented recently formulated novel approach to include the pp Coulomb force into the momentum space 3N Faddeev calculations. It is based on a standard formulation for short range forces and relies on a screening of the long-range Coulomb interaction. In order to avoid all uncertainties connected with an application of the partial wave expansion, unsuitable when working with long-range forces, we apply directly the 3-dimensional pp screened Coulomb t-matrix.

Using a simple dynamical model for the nuclear part of the interaction we demonstrated the feasibility of that approach. We provided analytical arguments and showed numerically that the physical elastic pd scattering amplitude has a well defined screening limit and therefore does not require renormalisation. Well converged elastic pd cross sections have been achieved at finite screening radii.

For the pd breakup we demonstrated that, contrary to the pd elastic scattering, where the resulting amplitudes do not require renormalisation, it is unavoidable to perform renormalisation of the pp half-shell t-matrices in order to get the physical breakup amplitude. Namely that amplitude has two contributions, one driven by the interaction in the pp subsystem and second in the np subsystem. Only the first part requires renormalisation.

We have shown that converged results for breakup can be achieved with finite screening radia.

We calculated contributions of different terms to the breakup cross section in QFS and SST configurations. The action of different contributions leads to an interference pattern, which is different for QFS and SST configurations. In our restricted dynamical model the pp Coulomb interaction brings the nd breakup cross sections close to the pd data for the QFS configuration. Also for the SST geometry in the vicinity of the space-star condition the pd theory is close to the pd data. However, further away on the S-curve the theory lies above the data.

In this first study the 3-dimensional screened pure Coulomb t-matrix was replaced by the screened Coulomb potential and only a small number of partial wave states for the NN interaction was taken into account.

In future studies the perturbative approximation for the 3-dimensional screened Coulomb t-matrix will be avoided and higher partial wave components of the nucleon-nucleon interaction will be included.

Acknowledgments

This work was supported by the Polish 2008-2011 science funds as the research project No. N N202 077435. It was also partially supported by the Helmholtz Association through funds provided to the virtual institute “Spin and strong QCD”(VH-VI-231) and by the European Community-Research Infrastructure Integrating Activity “Study of

Strongly Interacting Matter" (acronym HadronPhysics2, Grant Agreement n. 227431) under the Seventh Framework Programme of EU. The numerical calculations have been performed on the supercomputer cluster of the JSC, Jülich, Germany.

References

1. E.O. Alt, W. Sandhas, and H. Ziegelmann, Phys. Rev. **C17** (1978) 1981.
2. E.O. Alt and W. Sandhas, *Coulomb Interactions in Nuclear and Atomic Few-Body Collisions*, (eds. F.S. Levin and D. Micha, Plenum, New York, 1996), p.1.
3. E.O. Alt and M. Rauh, Phys. Rev. **C49** (1994) R2285.
4. E. O. Alt, A. M. Mukhamedzhanov, M. M. Nishonov, and A. I. Sattarov, Phys. Rev. **C65** (2002) 064613.
5. W. Glöckle, H. Witała, D. Hüber, H. Kamada, J. Golak, Phys. Rep. **274** (1996) 107.
6. E. Epelbaum, Prog. Part. Nucl. Phys. **57** (2006) 654; and references therein.
7. A. Kievsky, M. Viviani, and S. Rosati, Phys. Rev. **C52** (1995) R15.
8. A. Deltuva, A. C. Fonseca, and P. U. Sauer, Phys. Rev. **C72** (2005) 054004.
9. A. Deltuva, A. C. Fonseca, and P. U. Sauer, Phys. Rev. **C71** (2005) 054005.
10. E. Stephan et al., Phys. Rev. **C76** (2007) 057001.
11. G. Rauprich et al., Nucl. Phys. **A535** (1991) 313.
12. R. Großmann et al., Nucl. Phys. **A603** (1996) 161.
13. H. Patberg et al., Phys. Rev. **C53**, (1996) 1497.
14. M. Allet et al., Few-Body Syst. **20** (1996) 27.
15. J. Zejma et al., Phys. Rev. **C55** (1997) 42.
16. H. Witała, R. Skibiński, J. Golak, W. Glöckle, Eur. Phys. J. **A41** (2009) 369.
17. H. Witała, R. Skibiński, J. Golak, W. Glöckle, Eur. Phys. J. **A41** (2009) 385.
18. R. Skibiński, J. Golak, H. Witała, and W.Glöckle, Eur. Phys. J. **A40** (2009) 215.
19. H. Witała, W. Glöckle, H.Kamada, Phys. Rev. **C43** (1991) 1619.
20. W. Glöckle, The Quantum Mechanical Few-Body Problem, (Springer Verlag, 1983).
21. W.F. Ford, Phys. Rev. **133** (1964) B1616.
22. W.F. Ford, J. Math. Phys. **7** (1966) 626.
23. M. Yamaguchi, H. Kamada, and Y. Koike, Prog. Theor. Phys. **114** (2005) 1323.
24. J.R. Taylor, Nuovo Cimento **B23** (1974) 313.
25. M.D. Semon and J.R. Taylor, Nuovo Cimento **A26** (1975) 48.
26. L.P. Kok and H. van Haeringen, Phys. Rev. Lett. **46** (1981) 1257.
27. L.P. Kok and H. van Haeringen, Phys. Rev. **C21** (1980) 512.
28. J.C.Y. Chen and A.C. Chen, Advances of Atomic and Molecular Physics, (eds. D.R. Bates and J. Estermann, Academic, New York, 1972), Vol. 8.
29. R. Machleidt, F. Sammarruca, and Y. Song, Phys. Rev. **C53** (1996) R1483.
30. W. Grüebler et al., Nucl. Phys. **A398** (1983) 445.
31. H.R. Setze et al., Phys. Rev. **C71** (2005) 034006.